Chapter 5

Chapter 5. Tracing the anti-cancer mechanism of EFPO1 by the integrative approach of network pharmacology and experimental studies

5.1. Background

In Chapter 3, ethyl acetate fraction of DCM: Et crude extract of *P. osteratus* (EFPO1) showed good cytotoxic potential against panels of the cancer cell lines (following HFPO1), owing to the presence of a high abundance of alkaloids, along with significantly rich in polyphenolic and ergosterol class of myco-metabolites. The present chapter tries to explore the mechanistic pathway of EFPO1 against breast, blood, and lung cancer *via* network pharmacology along with experimental validation. Initially, we screened myco-metabolites quantified by LC-MS/MS and tentatively identified by LC-QTOF/MS, based on drug-likeness properties, targets of the myco-metabolites, and diseases (breast, blood, and lung cancer) were predicted from the online web server, and overlapping targets were further selected. Influential hub targets were identified by network analysis of PPI. Further, gene enrichment analysis of these target genes was performed *via* GO and KEGG. Molecular docking of the hub target with their selected myco-metabolites was studied. Predicted target genes involved in the KEGG pathway of cancer were further validated by immunoblot analysis of target protein expression of EFPO1 treated cell line, along with anti-tumor activity against Ehrlich ascites carcinoma (EAC) in Swiss albino mice.

5.2. Objectives

- Elucidation of mechanistic pathways of myco-metabolites of EFPO1 against the cancer using network pharmacology.
- Elucidation of mechanistic pathways of myco-metabolites of EFPO1 against the cancer using experimental methods.
    - *In-vitro* fluorescence imaging and immunoblot analysis of EFPO1 treated cancer cell line.
    - *In-vivo* anti-tumor activity of EFPO1 treated EAC (solid tumor) bearing Swiss albino mice, along with acute toxicity profile of EFPO1 in Swiss albino mice.

5.3. Experimental work

5.3.1. Preliminary work

Preliminary results on EFPO1 showed promising cytotoxicity against human blood, breast, and lung cancer cell lines (IC_{50} < 200 µg/mL), following HFPO1. As per LC-MS/MS-based quantification, EFPO1 was significantly rich in ergosterol and polyphenolic content (COUA, PA, QE, LUT, KAM, and API). LC-QTOF/MS untargeted myco-metabolite screening tentatively identified myco-metabolites with appreciable abundance in EFPO1 were alkaloids (SEN, CEP, and ACR), and fatty alcohol (AVO1). Hence, a total of eleven myco-metabolites were present in appreciable abundance in EFPO1.

5.3.2. Network pharmacology

5.3.2.1. In-silico drug-likeness screening

In-silico oral bioavailability and drug-likeness were determined by an online web server Swiss ADME (http://www.swissadme.ch/, accessed on 26 November 2021), using the procedure described in Chapter 4 (Section 4.3.2.1.). The myco-metabolites with oral bioavailability score > 0.5, following Lipinski's rule of five, were screened out for further analysis.

5.3.2.2. Compound-target prediction

Swiss target prediction, an online target prediction web server (http://www.swisstargetprediction.ch/, accessed on 28 November 2021) was used for the target prediction of identified myco-metabolites, using the methodology demonstrated in Chapter 4 (Section 4.3.2.2.).

5.3.2.3. Diseases-target prediction

Information related to target genes associated with the diseases: blood cancer, breast cancer, and lung cancer were obtained from MalaCards (https://www.malacards.org/#, accessed on 3rd December 2021) and DisGeNet (https://www.disgenet.org/search, accessed on 16th December 2021), using the protocol presented in Chapter 4 (Section 4.3.2.3.).

The target genes of the myco-metabolites from Swiss target prediction were compared with the target genes of the disease from MalaCards and DisGeNet individually, and the matched target genes were selected. These matched target genes from both database were again compared, and overlapping target genes were screened for analysis.

5.3.2.4. Protein-protein interaction

The protein-protein interaction was constructed by STRING web (https://string-db.org/, accessed on 28th January 2022) under the setting of confidence level between the protein-protein interaction as high as 0.9, using the method described in Chapter 4 (Section 4.3.2.4.). Nodes (protein) with no edges (interaction) were excluded, and the resultant protein-protein interaction network was further launched into the Cytoscape tool (Cytoscape; Version 3.8.2.) for the evaluation of topological features of the network.

5.3.2.5. Gene enrichment analysis

GO, and KEGG pathway of the resultant protein associated with protein-protein interaction (STRING) was analyzed by ShinyGO (http://bioinformatics.sdstate.edu/go/, accessed on 30th January 2022), using the methodology described in Chapter 4 (Section 4.3.2.5.). Both the analysis diminishes the redundancy of results and, thus, improvises the data prediction.

5.3.2.6. Network layout of compound-target

Graphical visualization of a network between myco-metabolites with target genes enriched in strong protein-protein interaction was constructed using the Cytoscape tool (Cytoscape; Version 3.8.2.), and network analysis was executed using the method demonstrated in Chapter 4 (Section 4.3.2.6.).

5.3.2.7. *In-silico* molecular docking

The molecular docking studies use the automated docking program AutoDock4.2 for studying the *in-silico* docking interaction of hub targets with their key myco-metabolites, using the protocols described in Chapter 4 (Section: 4.3.2.7.). The hub targets were ESR1, MAPK1, AKT1, BCL2L1 and FGFR for studying the *in-silico* molecular docking.

5.3.2.8. *In-silico* cancer multi-omic expression study & prognostic potential

Before *in-vitro* experimental validation, the mRNA and protein expression of the selected hub target (BCL2L1) in lung adenocarcinoma were analyzed by GEPIA (http://gepia2.cancer-pku.cn/#analysis, accessed on 2th February 2022) and UALCAN (http://ualcan.path.uab.edu/cgi-bin/ualcan-res.pl, accessed on 4th February 2022) respectively. UALCAN web server (http://ualcan.path.uab.edu/cgi-bin/ualcan-res.pl, accessed on 4th February 2022) was used for overall survival analysis of BCL2L1 in lung adenocarcinoma patients.

5.3.3. In-vitro experimental validation

5.3.3.1. Fluorescence microscopy

A549 cells were treated with 0, 50, 100, and 200 µg/mL concentrations of EFPO1 for 48 hours, using the procedure summarized in Chapter 4 (Section 4.3.3.1.).

5.3.3.2. Immunoblot analysis

Approximately 2×106 A549 cells/well were seeded and treated with different concentrations of EFPO1 (0, 50, 100, and 200 µg/mL) for 48 hours, using the protocol described in Chapter 4 (Section 4.3.3.2.).

5.3.4. *In-vivo* experimentation

5.3.4.1. Experimental animals

Prior to the experiment, Institutional Animal Ethics Committee approval (Protocol no. Dean/2021/IAEC/2553) was granted. The standard laboratory condition for nulliparous female Swiss albino mice (20-25 g) was same as described in Chapter 4 (Section 4.3.4.1.).

5.3.4.2. Acute toxicity assessment

Acute toxicity assay was conducted in accordance with OECD 425, using described methodology in Chapter 4 (Section 4.3.4.2.).

5.3.5. In-vivo anti-tumor efficacy in EAC (solid tumor) bearing Swiss albino mice

Protocol for the development of EAC (solid tumor) in Swiss albino mice was as per Chapter 4 (Section 4.3.5.). Mice bearing approximately 45 mm^3 tumor volume were scrutinized and randomized into 5 groups (5 animal/group) as follows. Group I: tumor-bearing mice (T); Groups II, III, and IV: tumor-bearing mice treated with a dose of 50 mg/kg p.o. (E1), 75 mg/kg p.o. (E2) and 100 mg/kg p.o. (E3) of EFPO1, respectively, for three alternate days for a period of 15 days; and Group V: tumor-bearing mice received the standard drug paclitaxel 10 mg/kg p.o. (S), for three alternate days for a period of 15 days. The control group receiving 0.5%w/v CMC (N) was also included in this study as Group VI. On the 0^{th} and 15^{th} days, tumor volume and body weight were recorded. Tumor volume was measured, using the formula described in Chapter 4 (Section 4.3.5.). At the end of the study, animals were humanely killed, and tumor weight was recorded.

5.4. Results and Discussion

5.4.1. Network pharmacology

5.4.1.1. *In-silico* drug-likeness screening

The myco-metabolites quantified and tentatively identified were evaluated based on the drug-likeness properties following Lipinski's rule of 5. Remarkably, all the tentatively identified molecules (11) pass Lipinski's rule of 5 with a bioavailability score > 0.5 as shown in Table 5.1. One compounds (ERG) violated one of the rules of Lipinski with MLogP greater than 5, hence overruled.

Table 5.1. Drug-likeness properties of tentatively identified myco-metabolites.

Molecule	MW	HBA	HBD	MlogP	Lipinski violations	Bioavailability Score
COU	164.16	3	2	1.28	0	0.85
PA	154.12	4	3	0.4	0	0.56
QE	302.24	7	5	-0.56	0	0.55
LUT	286.24	6	4	-0.03	0	0.55
KEMP	286.24	6	4	-0.03	0	0.55
API	270.24	5	3	0.52	0	0.55
CEP	466.61	6	2	2.84	0	0.55
SEN	335.39	6	1	1.43	0	0.55
AVO1	326.47	4	2	3.07	0	0.55
ACR	323.34	6	5	-0.57	0	0.55
ERG	396.65	1	1	6.33	1	0.55

MW: Molecular weight; HBA: Hydrogen bond acceptor; HBD: Hydrogen bond donor

5.4.1.2. Compound-target prediction

From 11 tentatively identified myco-metabolites, 9 myco-metabolites were assigned predicted targets. Whereas for AVO1 and ACR, no similar actives were found; hence no targets were predicted. Uniprot accession ID and the gene symbol of the predicted target were preserved for further exploration. The list of the predicted target for the individual compound is shown in the Table 5.2.

Table 5.2. List of the predicted targets for quantified and tentatively identified myco-metabolites.

COUA	PA	QE	LUT	KEMP	API	CEPH	SEN	ERG
AKR1B1	CA2	NOX4	NOX4	NOX4	GPR35	RBBP9	CYP19A1	VDR
CA2	CA7	AVPR2	AKR1B1	AKR1B1	ERBB2	ADRA2A	CA7	PTPN1
CA7	CA1	AKR1B1	CDK5R1 CDK5	XDH	AKR1B1	ADRA2C	ABCC1	GLRA1
ESR2	CA6	XDH	XDH	TYR	CCND1 CDK4	ADRA1A	HSD17B1	NR1H3
CA1	CA12	MAOA	MAOA	FLT3	PDGFRB	ABCB1	CA12	AR
CA3	CA14	IGF1R	FLT3	CA2	FLT4	KCNN1	SHBG	NPC1L1
CA6	CA9	FLT3	CA2	ALOX5	IGF1R	KCNN3	CA4	
CA12	CA4	CYP19A1	CCNB3 CDK1 CCNB1 CCNB2	CA7	INSR	KCNN2	CYP1B1	
CA14	CA3	EGFR	ALOX5	HSD17B2	EGFR	SLC18A2	CBR1	
CA9	CA5B	F2	ADORA1	ABCC1	CA2	DPP4	ESR1	
CA4	CA5A	CA2	CA7	HSD17B1	CDK2 CCNA1 CCNA2	DRD2	ESR2	
CA5B	CA13	PIM1	GLO1	AHR	AURKB	SLC6A4	PTGS1	
	FUT7	ALOX5	APP	CA12	CA7	SLC6A3	MAOB	
MIF	SQLE	AURKB	SYK	ESRRA	CA1	PARP1	ADORA1	
ALOX5	LDHA	DRD4	GSK3B	ABCB1	GSK3B	DRD1	ADORA3	
MMP9	LDHB	ADORA1	PARP1	CYP1B1	SRC	SIGMAR1	ABCG2	
MMP1	TTR	CA7	TTR	ABCG2	PTK2	OPRK1	TAS2R31	
MMP2	ESR2	GLO1	MMP9	ADORA1	KDR	KCNH2	AKR1C3	
PTPN1	COMT	MPO	CA12	CA4	PLK1	OPRM1	PLA2G1B	
AKR1B10	BCL2L1	PIK3R1	MMP2	ACHE	CA6	ACHE	GRM5	
HCAR2	IGF1R	ADORA2A	CA4	MAOA	CA12	BCHE	CES1	
TLR4	ALK	DAPK1	MMP12	GLO1	CA14	DRD3	PPARG	
CA13	SERPINE1	PYGL	CD38	SYK	CA9	ADRA1B	CES2	
F3	AKR1C3	CA1	CYP1B1	GSK3B	CSNK2A1	OPRD1	SLC5A2	
HSD11B1	GPR35	GSK3B	ABCG2	MMP9	MET	HTR1A	MMP12	
TRPA1	ALB	SRC	AKR1B10	MMP2	CA4	DRD4	POLB	
ESR1		PTK2	TNKS2	ALOX15	PLK4	ADRB1	MMP13	
PGR		HSD17B2	TNKS	ALOX12	CA13	TBXA2R	PLA2G2A	
AKR1C3		KDR	TOP1	PTPRS	TEK	ADRB2	PLA2G5	
		MMP13	ARG1	ADORA2A	AKT1	ADRA1D	PLA2G10	
		MMP3	PTPRS	CDK5R1 CDK5	AURKA	MTNR1B	BACE1	
		CA3	ABCC1	CCNB3 CDK1 CCNB1 CCNB2	CA5A	HRH3	CHRNA7	
		ALOX15	HSD17B1	ARG1	BACE1	JUN	KLK1	

Table 5.2. Continued

COUA	PA	QE	LUT	KEMP	API	CEPH	SEN	ERG
		ABCC1	ACHE	GPR35	MAP3K8	MAOA	KLK2	
		PLK1	CDK6	ESR2	BRAF	DHCR7	RXRA	
		CA6	ABCB1	DAPK1	EPHB4	DRD5	SERPINE1	
		CDK1	HSD17B2	MPG	HSPA1A	HTR7	SRC	
		MMP9	CYP19A1	SLC22A12	NUAK1	F3	CA2	
		CA12	ESR2	TTR	SQLE	HTR2A	CA1	
		MMP2	ADORA2A	AKR1B10	FGR	ESR1	HSD17B14	
		PKN1	CSNK2A1	TNKS2	LYN	ESR2	KIT	
		CA14	ALOX15	TNKS	GSR	MTNR1A	KDR	
		CA9	ALOX12	CDK6	TNNC1 TNNT2 TNNI3	OPRL1	FGFR1	
		CSNK2A1	ESR1	CDK2	XDH	CHRM4	MET	
		ALOX12	PTGS2	CYP19A1	DAO	ADRB3	CA3	
		MET	CFTR	CSNK2A1	PTGS2	CHRNA7	CA6	
		CA4	AMY1A	EGFR	ESR1	ABCC1	CA13	
		NEK2	GRK6	AVPR2	ESR2	PRKCI	CA5B	
		CXCR1	CA1	IGF1R	MAOA	HTR2B	CA5A	
		CAMK2B	CA9	F2	HSD17B3	HTR2C	NQO2	
		ALK	CDK2	PIM1	PTPN1	TACR1	CTSB	
		AKT1	TERT	AURKB	ALOX5	CHRNA4 CHRNB2	NOX4	
		ABCB1	CDK1	DRD4	CBR1	NPY5R	AKR1B1	
		NEK6	TYR	MPO	CDK5R1 CDK5	PARP2	CLK1	
		PLA2G1B	AHR	PIK3R1	CES2	HCRTR1	DYRK1B	
		CA5A	ESRRA	PYGL	CA5B	ROCK1	BCHE	
		BACE1	GPR35	CA1	SNCA	CCR2	CA9	
		CYP1B1	AVPR2	SRC		HCRTR2	ESRRA	
		AXL	IGF1R	PTK2		DPP8	ESRRB	
		ABCG2	EGFR	KDR		HRH1	CDK5R1 CDK5	
		NUAK1	F2	MMP13		SLC47A1	IGF1R	
		AKR1C2	PIM1	MMP3		HSD11B1	INSR	
		AKR1C1	AURKB	CA3		ROCK2 ROCK1	DYRK1A	
		AKR1C3	DRD4	PLK1		RPS6KB1	HSD17B2	
		AKR1C4	MPO	CA6		AURKA	IGFBP3	
		CA13	PIK3R1	CDK1		DPP7	MMP2	
		AKR1A1	DAPK1	PKN1		CHEK1	YWHAG	
		GPR35	PYGL	CA14		WEE1	SIRT2	
		MAPT	SRC	CA9		SLC6A2	F3	
		KDM4E	PTK2	MET		AURKB	PTGER1	
		TOP2A	KDR	NEK2		MAPK1	PTGER2	
		INSR	MMP13	CXCR1		CSF1R	PTGER3	
		ACHE	MMP3	CAMK2B		CHRNB4 CHRNA2	BCL2L1	
		MYLK	CA3	ALK		GRIN2A GRIN1	PIK3CB	
		SYK	PLK1	AKT1		FAAH	CYP2C9	

Table 5.2. Continued

COUA	PA	QE	LUT	KEMP	API	CEPH	SEN	ERG
		PIK3CG	CA6	NEK6		KDM1A	CYP3A4	
		APEX1	PKN1	PLA2G1B		KDM5C	PIK3CA	
		PTPRS	CA14	CA5A		KDM4B	VCP	
		ESR2	MET	BACE1		KDM5B	PGF	
		MPG	NEK2	AXL		KDM4A	VEGFA	
		SLC22A12	CXCR1	NUAK1		ERG	EDNRA	
		CDK5R1 CDK5	CAMK2B	AKR1C2		CXCR4	ERN1	
		CCNB3 CDK1 CCNB1 CCNB2	ALK	AKR1C1		LTA4H	MMP3	
		ARG1	AKT1	AKR1C3		PDK1	APP	
		CDK6	NEK6	AKR1C4		SMYD2	GSK3B	
		CDK2	PLA2G1B	CA13		PIK3CD	BCL2	
		TYR	CA5A	AKR1A1		PDGFRB	MMP9	
		HSD17B1	BACE1	APP		MELK	WEE1	
		AHR	AXL	PARP1		MAOB	LCK	
		ESRRA	NUAK1	MMP12		NPBWR1	SYK	
		APP	AKR1C2	CD38		KDM3A	CCNE1 CDK2	
		PARP1	AKR1C1	TOP1		ABL1	CCNE1 CDK3	
		TTR	AKR1C3	ESR1		KIT	CDK4	
		MMP12	AKR1C4	PTGS2		KDM2A	AURKA	
		CD38	CA13	CFTR		INSR	SNCA	
		AKR1B10	AKR1A1	PFKFB3		PDGFRA	ALOX12	
		TNKS2	PFKFB3	AMY1A		RET	HNF4A	
		TNKS	PLG	GRK6		JAK3		
		TOP1	KDM4E	TERT		PDPK1		
		TERT	AR	MAPT		KDR		

The pink box represents duplicate target genes.

5.4.1.3. Diseases-target prediction

MalaCards database predicted an aggregate of 1056, 150, and 876 target genes for BC, HC, and LC, respectively. Comparably, 95, 80, and 16 target genes for BC, HC, and LC overlapped with the myco-metabolites-target gene, respectively, hence resulting in the procurement of a total of 191 target genes, as shown in Table 5.3. Further, the exclusion of duplicate target genes from 191 target genes yields a total of 111 target genes as shown in the Venn diagram (Figure 5.1.a).

Table 5.3. Overlapped myco-metabolites-target genes with MalaCards diseases-target genes.

BC	LC	HC
CA9	IGF1R	FLT3
ABCG2	EGFR	KDR
MET	AURKB	ABCC1
PTGS2	PIK3R1	ALK
CDK2	DAPK1	ABCB1
AKT1	SRC	SYK
CCNB2	PTK2	TOP1
FGFR1	KDR	KIT
IGF1R	MMP13	VEGFA
CYP19A1	MMP3	BCL2
EGFR	ABCC1	PDGFRB
CA2	PLK1	CSF1R
AURKB	CDK1	ABL1
PIK3R1	MMP9	CXCR4
GSK3B	MMP2	JAK2
SRC	CA9	FGFR1
PTK2	MET	
KDR	NEK2	
MMP13	ALK	
MMP3	AKT1	
ABCC1	ABCB1	
PLK1	PLA2G1B	
CDK1	CYP1B1	
MMP9	AXL	
MMP2	ABCG2	

Table 5.3. Continued

BC	LC	HC
CSNK2A1	AKR1C1	
NEK2	TOP2A	
ALK	ACHE	
ABCB1	PIK3CG	
CYP1B1	APEX1	
AXL	ESR2	
AKR1C3	CDK5	
TOP2A	CCNB1	
INSR	CDK6	
MYLK	CDK2	
SYK	HSD17B1	
PIK3CG	PARP1	
APEX1	MMP12	
ESR2	TOP1	
CCNB1	TERT	
CDK6	BCL2L1	
HSD17B1	ALB	
AHR	ESR1	
ESRRA	MIF	
PARP1	MMP1	
TOP1	TLR4	
TERT	CBR1	
BCL2L1	KIT	
SERPINE1	AURKA	
LDHA	PPARG	
ESR1	RXRA	
MMP1	FGFR1	
PGR	CTSB	
SHBG	DYRK1B	
KIT	IGFBP3	
WEE1	PIK3CB	
AURKA	CYP3A4	
PPARG	PIK3CA	
PLA2G10	VEGFA	
NQO2	BCL2	
CTSB	CCNE1	
IGFBP3	PTGS2	
PIK3CB	PDGFRB	
CYP3A4	JUN	
PIK3CA	PRKCI	
VEGFA	ROCK1	
BCL2	RPS6KB1	
CCNE1	CHEK1	
VDR	MAPK1	

Table 5.3. Continued

BC	LC	HC
PDGFRB	JAK3	
JUN	RET	
ROCK1	PDGFRA	
ROCK2	PDK1	
RPS6KB1	CXCR4	
CHEK1	MAPK14	
MAPK1	PTK2B	
CSF1R	IDH1	
RET	CDK6	
PDGFRA	FGFR3	
ABL1	FLT1	
PIK3CD	MAP2K1	
CXCR4		
KDM5B		
KDM4B		
MAPK14		
PTK2B		
IDH1		
ALDH1A1		
JAK1		
CDK6		
FGFR3		
FLT1		
FLT3		
PSEN2		
MAP2K1		
HMGCR		

The pink box represents duplicate target genes.

DisGeNet database retrieved a total of 19897, 18183, and 10845 target genes for BC, HC, and LC, respectively. Collectively, 591 target genes consisting of 224, 187, and 180 myco-metabolites-target genes matched with BC, HC, and LC diseases-target genes as shown in Table 5.4. After removing duplicate target genes from 591 target genes, 247 target genes were left out, as shown in the Venn diagram (Figure 5.1.b).

Table 5.4. Overlapped myco-metabolites-target genes with DisGeNet diseases-target genes.

BC	LC	HC
Q9NPH5	Q9NPH5	Q9NPH5
P30518	P15121	P15121
P15121	P47989	P21397
P47989	P08069	P08069
P21397	P36888	P36888
P08069	P11511	P11511
P36888	P00533	P00533
P11511	P00918	P00734
P00533	P11309	P00918
P00734	Q96GD4	P11309
P00918	P21917	P09917
P11309	P05164	Q96GD4
P09917	P27986	Q04760
Q96GD4	P53355	P05164
P21917	P00915	P27986
P30542	P49841	P29274
Q04760	P12931	P53355
P05164	Q05397	P49841
P27986	P35968	P12931
P53355	P45452	Q05397
P00915	P08254	P35968
P49841	P16050	P45452
P12931	P33527	P08254
Q05397	P53350	P16050
P37059	P06493	P33527
P35968	P14780	P53350
P45452	O43570	P06493
P08254	P08253	P14780
P16050	Q16790	O43570
P33527	P68400	P08253
P53350	P08581	Q16790
P06493	P51955	P68400
P14780	P25024	P18054
O43570	Q9UM73	P08581
P08253	P31749	P51955
Q16790	P08183	P25024
P68400	P04054	Q9UM73
P18054	P56817	P31749
P08581	Q16678	P08183
P51955	P30530	Q9HC98
P25024	Q9UNQ0	P04054
Q13554	P52895	Q16678

Table 5.4. Continued

BC	LC	HC
Q9UM73	Q04828	P30530
P31749	P42330	Q9UNQ0
P08183	P14550	O60285
Q9HC98	P10636	Q04828
P04054	O14746	P42330
P35218	P11387	P17516
Q16678	O95271	P14550
P30530	Q9H2K2	P10636
Q9UNQ0	O60218	O14746
O60285	P28907	P11387
P52895	P39900	O95271
Q04828	P02766	P28907
P42330	P09874	P09874
P17516	P05067	P39900
Q8N1Q1	P11474	P02766
P14550	P35869	P35869
Q9HC97	P14061	P05067
P10636	P24941	P11474
O14746	Q00534	P14679
P11387	P05089	P24941
O95271	P06213	P06213
Q9H2K2	P22303	Q00534
O60218	P43405	P05089
P28907	Q92731	P22303
P39900	P29372	Q15078
P02766	Q15078	P43405
P09874	O95067	Q92731
P05067	P14635	P14635
P11474	P11388	P11388
P35869	Q15746	P48736
P14061	P48736	P27695
P14679	P27695	Q07817
P24941	Q14534	P05121
Q00534	Q07817	Q11130
P06213	P05121	P00338
P22303	Q11130	P21964
P43405	P00338	P02768
Q92731	P07195	P18031
P29372	P21964	P13726
Q15078	P02768	P03372
O95067	P18031	P14174
P14635	P13726	P03956
P11388	P03372	O00206
Q15746	P14174	P06401

Table 5.4. Continued

BC	LC	HC
P48736	P03956	P04278
P27695	O00206	P23219
Q14534	O75762	P16152
Q07817	P06401	P41594
P05121	P23219	P23141
P00338	P0DMS8	P37231
P07195	P16152	P39877
P21964	P23141	P19793
P02768	P37231	P11362
P18031	P31639	P16083
P13726	P06746	P07858
P28845	P14555	O95718
P03372	O15496	Q13627
P14174	P36544	P17936
P03956	P06870	P41235
Q8TDS4	P20151	Q00526
O00206	P19793	P24864
P06401	P11362	P06239
P04278	P07858	P10415
P23219	Q9Y463	O75460
P16152	Q13627	P25101
P27338	P17936	P15692
P37231	P41235	P49763
P31639	P11802	P42336
P06746	Q00526	P08684
P14555	P24864	P11712
O15496	P06239	P42338
P06870	P10415	Q8IXJ6
P20151	P25101	O00748
P19793	P15692	P10721
P11362	P49763	P06276
P16083	P55072	P30291
P07858	P42336	O14965
P49759	P08684	P37840
Q9Y463	P11712	P35354
O95718	P42338	P13569
Q13627	Q8IXJ6	P43250
P17936	P61981	Q16875
P41235	P10721	P10275
P11802	P06276	P11473
Q00526	P30291	Q13133
P24864	O14965	P04626
P10415	P37840	P11802
O75460	P35354	P35916

Table 5.4. Continued

BC	LC	HC
P25101	P13569	P20248
P15692	P04745	P78396
P49763	Q16875	O00444
P55072	P10275	Q02763
P42336	P11473	P41279
P08684	P23415	P15056
P11712	P04626	P54760
P42338	P35916	P0DMV8
P43115	P20248	P09769
P43116	P78396	P07948
Q8IXJ6	O00444	P19429
O00748	Q02763	P09619
P10721	P41279	P35348
P06276	P15056	Q92952
P30291	P54760	P27487
O14965	P0DMV8	P14416
P37840	P09769	P41145
P35354	P07948	Q12809
P13569	P00390	P35372
Q16875	P19429	P35462
P10275	P09619	P08908
P11473	P35348	P07550
P04626	Q05940	P52333
P35916	P27487	P07949
P20248	P14416	P16234
P78396	Q01959	P00519
O00444	P21728	Q9Y4C1
Q02763	P35372	Q14680
P41279	P21731	O00329
P15056	P07550	Q9NRG4
P54760	O15530	Q15118
P0DMV8	P52333	P61073
P09769	P07949	O75164
P07948	P16234	P11308
P00390	Q9Y2K7	Q9UGL1
P63316	P00519	O60341
P09619	Q9Y4C1	P07333
P08913	Q14680	P28482
P18825	O00329	O14757
P35348	Q15118	P23443
Q9UGI6	P61073	P49286
P27487	O75164	Q6V1X1
P14416	P11308	P41597
P31645	Q9UGL1	Q13464

Table 5.4. Continued

BC	LC	HC
Q01959	O94953	Q9UGN5
P21728	O60341	Q15761
Q99720	Q15822	P25103
Q12809	P07333	P36544
P35372	P28482	P48039
P35462	P23975	P05412
P08588	O14757	
P21731	P23443	
P07550	Q13464	
P25100	P41597	
O15530	P41743	
P52333	P48039	
P07949	P05412	
P16234		
Q9Y2K7		
P00519		
Q9Y4C1		
Q14680		
O00329		
Q9NRG4		
Q15118		
P61073		
O75164		
P11308		
Q9UGL1		
O94953		
P41229		
O60341		
O00519		
Q05586		
P07333		
P28482		
P23975		
O14757		
P23443		
Q13464		
P49286		
Q9Y5N1		
P35367		
Q6V1X1		
P41597		
Q9UGN5		
Q15761		
P25103		

Table 5.4. Continued

BC	LC	HC
P13945		
P48039		
P28223		
P05412		
P21918		
P34969		

The pink box represents duplicate target genes.

Finally, 111 target genes from MalaCards and 247 target genes from DisGeNet were matched, resulting in the overlapping of 111 target genes from both the database, as shown in the Venn diagram (Figure 5.1.c). This overlapped 111 target genes may be regarded as the most influential target for BC, HC, and LC.

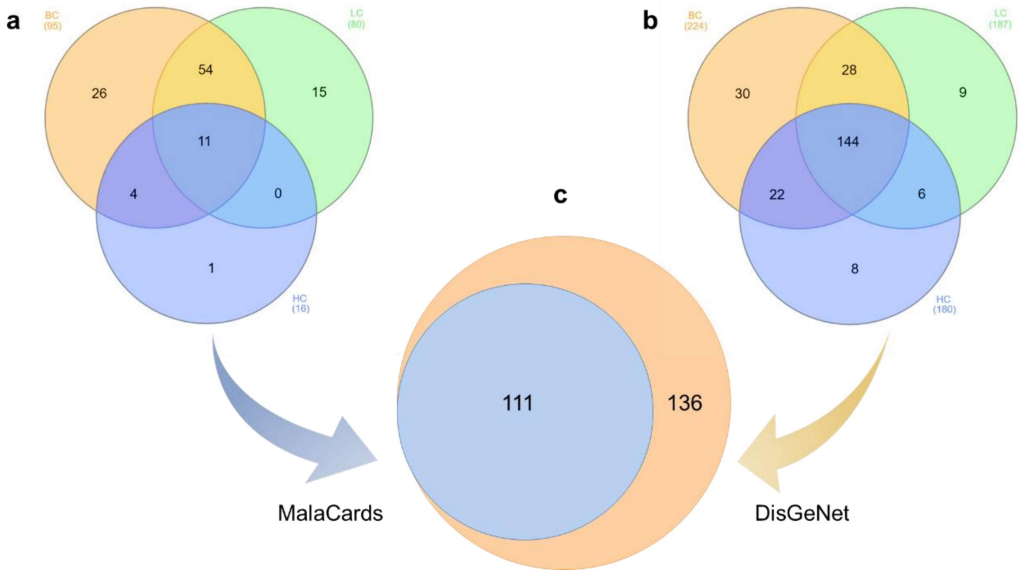

Figure 5.1. Venn diagram of overlapping myco-metabolites-target genes (a) with Malacards database for BC, HC, and LC (b) with DisGeNet database for BC, HC and LC, and (c) altogether from MalaCards and DisGeNet database.

5.4.1.4. Protein-protein interaction

The STRING protein-protein interaction of 111 target genes is shown in Figure 5.2. The interacted STRING protein-protein network has 111 nodes (proteins) connected by 356 edges (interaction) with an average local clustering coefficient of 0.522 and an average node degree of 6.41. The p-value (PPI enrichment) was found to be less than 1, thus

suggesting that the resultant network has significantly more interaction than excepted. With a confidence level of 0.9, 17 target genes, namely DYRK1B, CA9, CTSB, IDH1, CA2, MMP13, PSEN2, DAPK1, ESRRA, ACHE, PTGS2, MMP12, KDM5B, PLA2G10, PDK1, NQO2, and SERPINE1 were omitted, owing to zero-degree node interaction. On account of non-connectivity with a central hub, four target genes (SHBG, ALB, ABCC1, and ABCG2) with one-degree node connection, their average short path length, and closeness centrality as one were further excluded from the study. The protein-protein interaction of the resultant 90 target genes is shown in Figure 5.2.

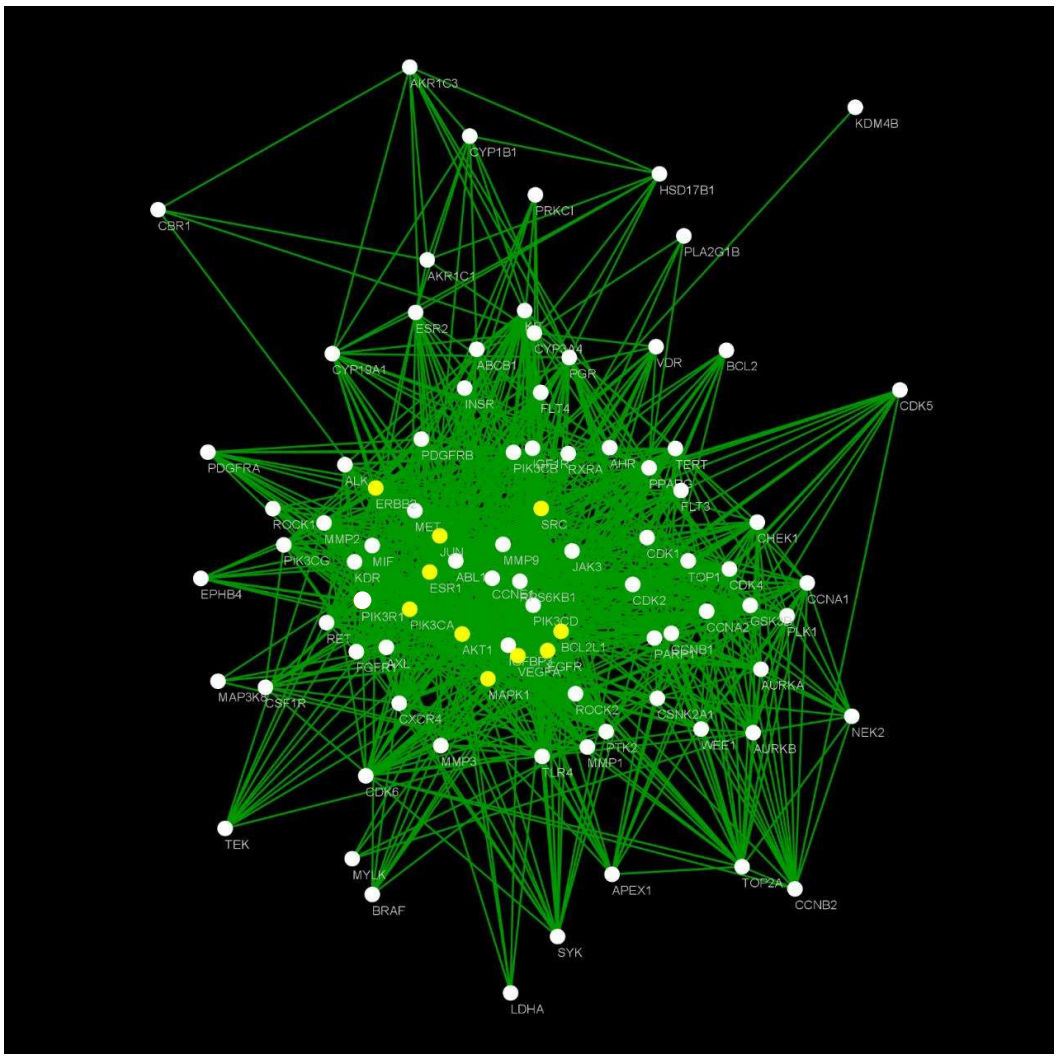

Figure 5.2. Protein-Protein interaction of 90 target genes. Yellow nodes represent the top 10 nodes based on degree.

The topological analysis consisting of degree, closeness centrality, and betweenness centrality of target genes are featured in the Table 5.5.

Table 5.5. Topological analysis of protein-protein interaction of 90 target genes.

Target genes	Degree	Betweenness centrality	Closeness centrality
AKT1	65	0.066465	0.777778
VEGFA	64	0.049461	0.771186
EGFR	64	0.057869	0.771186
SRC	63	0.053723	0.764706
ESR1	58	0.095127	0.733871
JUN	57	0.035905	0.728
ERBB2	54	0.029733	0.710938
PIK3CA	53	0.032048	0.705426
MAPK1	49	0.035934	0.684211
BCL2L1	43	0.011164	0.65
PIK3R1	42	0.015237	0.65
MMP9	39	0.01101	0.636364
CDK4	39	0.01052	0.631944
CCNB1	36	0.008411	0.619048
PTK2	35	0.009854	0.619048
PIK3CB	34	0.007747	0.602649
KDR	34	0.005809	0.606667
CCNA2	34	0.007018	0.610738
PPARG	34	0.014507	0.610738
CDK2	33	0.007052	0.606667
PGR	33	0.018506	0.610738
CXCR4	32	0.004943	0.594771
IGF1R	32	0.003972	0.606667
CDK1	32	0.009049	0.602649
CHEK1	32	0.008874	0.602649
MMP2	32	0.005232	0.602649
KIT	31	0.003882	0.598684
CCNE1	31	0.005232	0.598684
TERT	31	0.004952	0.598684
PARP1	30	0.00375	0.594771
CDK6	29	0.00424	0.590909
RPS6KB1	28	0.004043	0.590909
PIK3CD	28	0.004198	0.572327
GSK3B	27	0.003049	0.583333
MET	27	0.001909	0.579618
TLR4	27	0.005391	0.565217
TOP2A	26	0.004312	0.579618
PDGFRB	25	0.001949	0.56875

Table 5.5. Continued

Target genes	Degree	Betweenness centrality	Closeness centrality
FGFR1	25	0.001582	0.575949
ABL1	25	0.003268	0.575949
PLK1	24	0.004131	0.572327
PIK3CG	23	0.00142	0.548193
RET	22	0.001045	0.561728
AURKA	22	0.002667	0.565217
TOP1	21	0.001554	0.54491
CYP19A1	21	0.005865	0.561728
ESR2	21	0.016651	0.561728
CCNA1	20	0.001756	0.535294
WEE1	20	0.002898	0.541667
INSR	19	0.002414	0.551515
AURKB	19	0.003328	0.502762
FLT4	19	5.96E-04	0.52907
ALK	18	4.27E-04	0.548193
JAK3	18	0.001692	0.532164
CYP3A4	18	0.013458	0.541667
SYK	18	7.05E-04	0.532164
IGFBP3	17	0.002043	0.541667
FLT3	17	0.001845	0.532164
MMP1	16	2.61E-04	0.538462
CDK5	16	0.001108	0.532164
CCNB2	16	3.85E-04	0.446078
AHR	15	0.001593	0.535294
ABCB1	15	0.002084	0.538462
MMP3	15	2.48E-04	0.535294
PDGFRA	15	3.58E-04	0.535294
APEX1	15	0.001142	0.538462
VDR	14	6.58E-04	0.52907
AXL	14	0.001867	0.52
CSF1R	14	1.89E-04	0.514124
TEK	12	8.94E-05	0.511236
RXRA	12	0.001161	0.532164
ROCK1	12	3.12E-04	0.514124
CSNK2A1	11	3.67E-04	0.511236
CYP1B1	11	0.001829	0.469072
NEK2	11	1.56E-04	0.455
AKR1C3	9	0.001823	0.466667
EPHB4	9	1.22E-04	0.491892
ROCK2	9	2.21E-04	0.505556
BRAF	9	3.56E-05	0.505556
BCL2	9	4.05E-04	0.511236
HSD17B1	9	0.001074	0.459596

Table 5.5. Continued

Target genes	Degree	Betweenness centrality	Closeness centrality
MIF	8	1.22E-04	0.494565
LDHA	6	3.05E-05	0.489247
AKR1C1	6	3.17E-04	0.382353
PRKCI	6	0	0.466667
PLA2G1B	5	3.28E-05	0.497268
MYLK	5	1.92E-04	0.494565
MAP3K8	4	0	0.47644
CBR1	4	4.96E-04	0.441748
KDM4B	1	0	0.425234

The yellow-filled cells are the top 10 target genes.

The top 10 target genes based on topological analysis were AKT1, VEGFA, EGFR, SRC, ESR1, JUN, ERBB2, PIK3CA, MAPK1, and BCL2L1 (indicated with yellow nodes in Figure 5.2.). With the considerably high value of the degree, closeness centrality, and betweenness centrality, these target genes can be considered as nodes with high interaction, hub nodes, and nodes with potential control, respectively.

5.4.1.5. Gene enrichment analysis

The Shiny GO operating interface for GO enrichment was set at p-value ≤ 0.05, *i.e.*, based on FDR, for analyzing target genes in three arenas: GO biological, GO cellular, and GO molecular. FDR represents how likely the enrichment is by chance. The obtained top 10 GO biological, GO cellular and GO molecular processes encompassing target genes are shown in Figure 5.3. Similar operating settings were used for the KEGG pathway in the Shiny GO webserver. The top 10 enriched pathways involving target genes are represented in a dot plot, as shown in Figure 5.4. Out of 90 target genes, 44 target genes were involved in KEGG pathways of cancer, as shown in Figure 5.5. These 44 genes were majorly related to the estrogen signalling pathway, PPAR signalling pathway, tyrosine kinase signalling pathway, downstream signalling pathway: the MAPK pathway, PI3K-AKT pathway, and JAK-STAT pathway, Wnt signalling pathway, CDK, and Bcl-2/Bcl-XL. Over and above involvement in the pathway of cancers, these target

genes also contribute to other pathways (which were indirectly linked to the pathway of cancer); these pathways were PI3K-AKT signalling pathway, EGFR tyrosine kinase inhibitor resistance pathway, Ras signalling pathway, focal adhesion, proteoglycans in cancer pathway, Rap1 signalling pathway, central carbon metabolism in cancer, and chemical carcinogenesis., as shown in Figure 5.4.

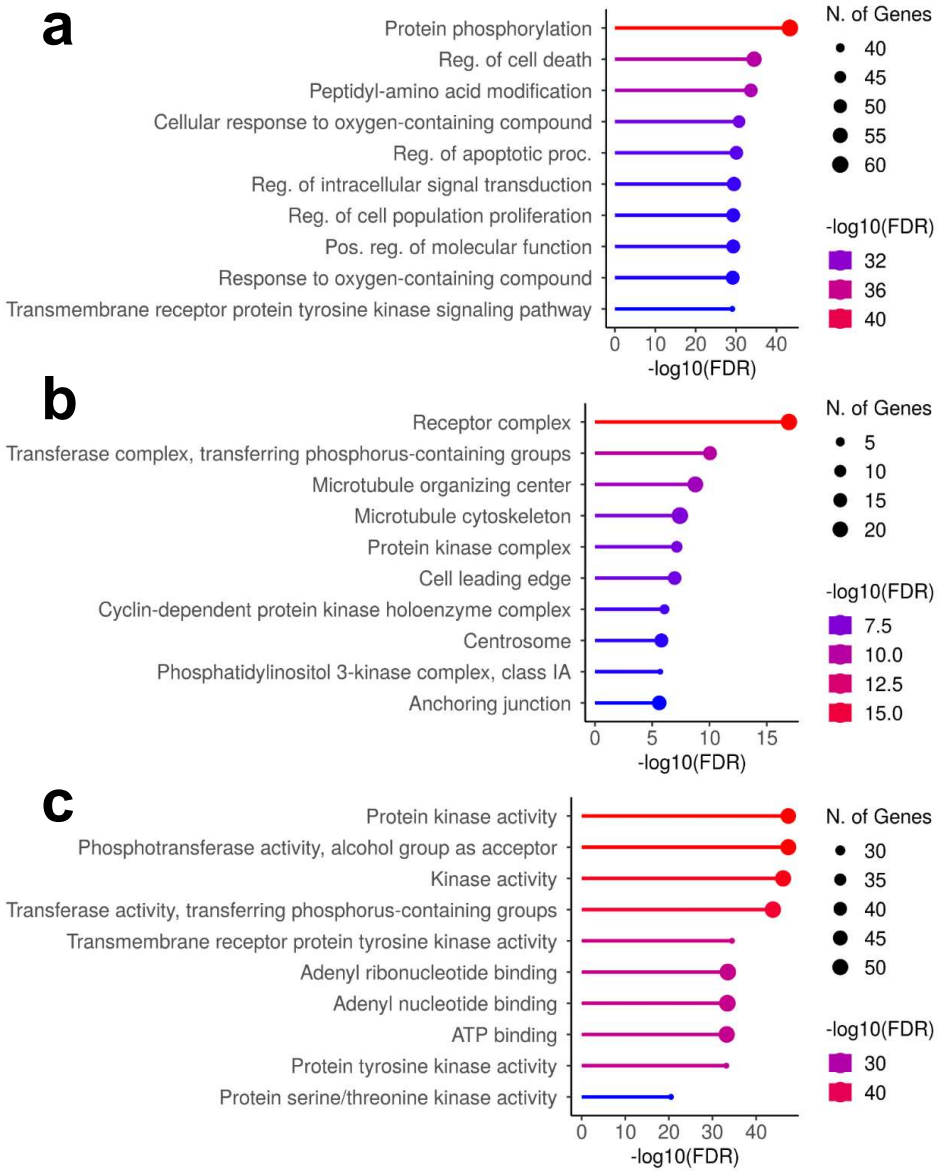

Figure 5.3. Top 10 Gene ontology enrichment in three arenas (a) biological process (b) cellular component, and (c) molecular function of 90 target genes.

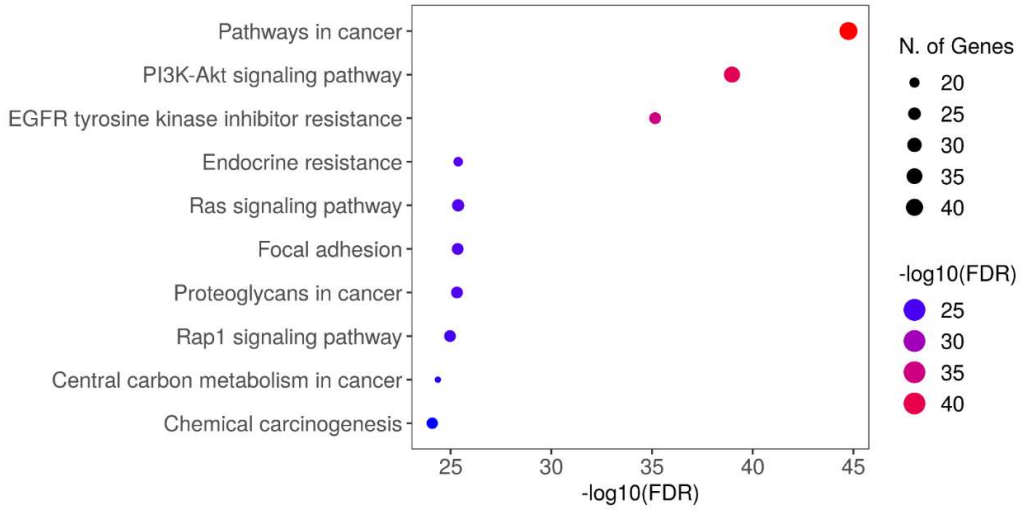

Figure 5.4. Dot plot of top 10 KEGG pathways of 90 target genes.

5.4.1.6. Network layout of compound-target

The obtained network consists of 100 nodes (1 EFPO1 node, 9 myco-metabolites nodes, and 90 target genes nodes) interconnected by 461 edges (interaction) (Figure 5.6.). Based on degree, which indicates the number of interactions of particular nodes, the metabolites were ranked. LUT stands out with 89 degrees, followed by KAM with 87, SEN with 60, and CEP with 43.

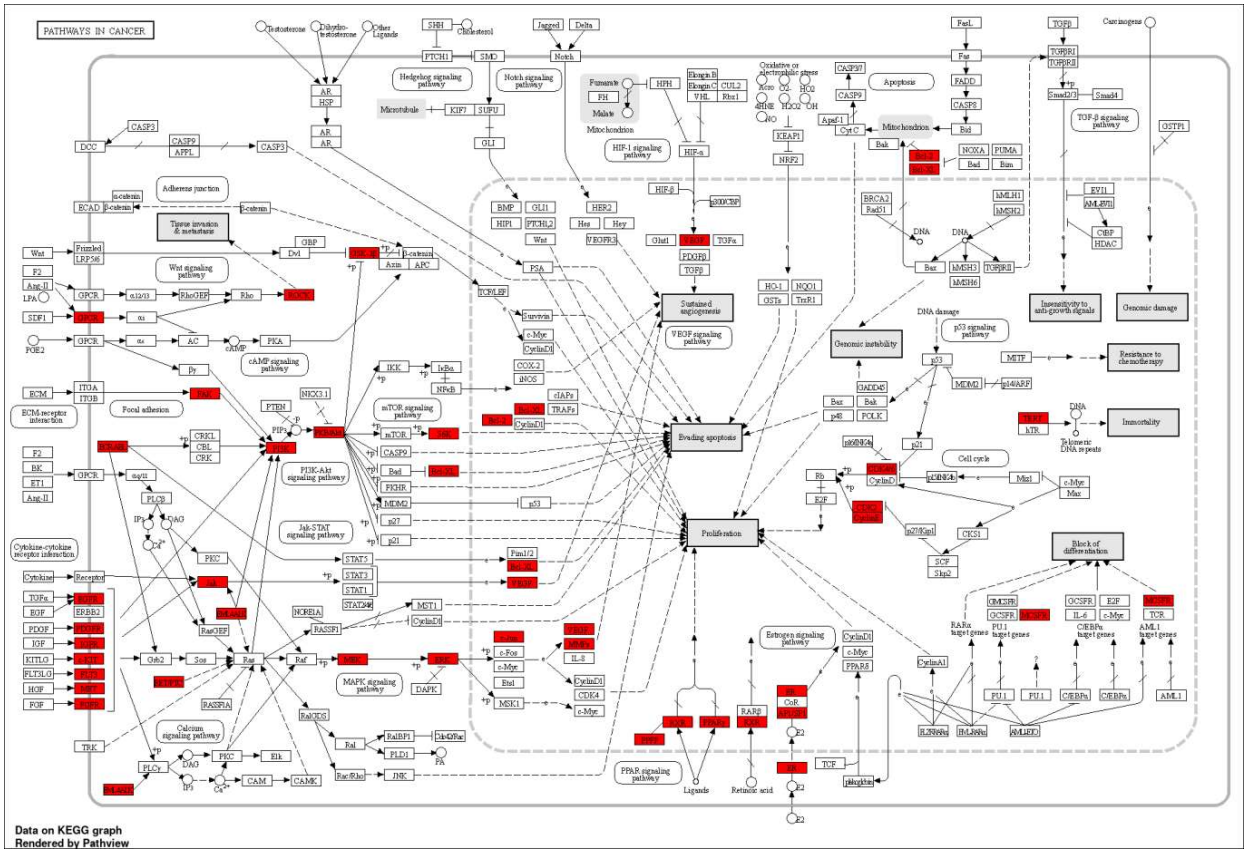

Figure 5.5. Target genes involved in KEGG's pathway of cancer.

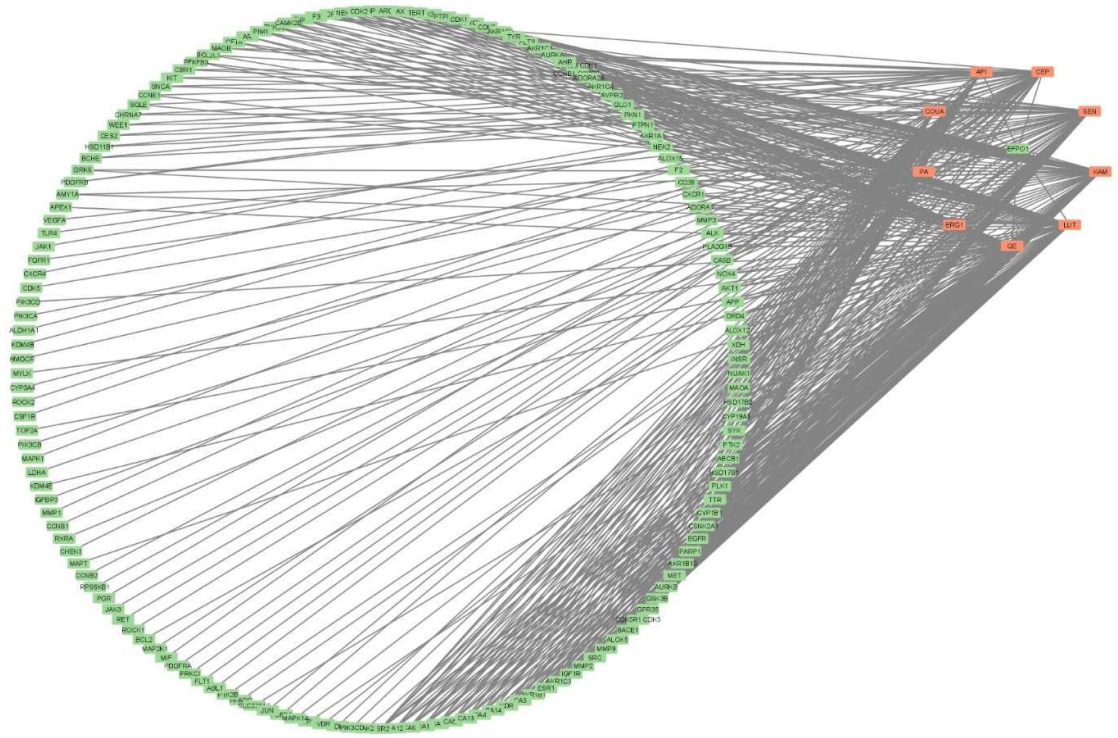

Figure 5.6. Interaction between myco-metabolites of EFPO1 with 90 target genes.

5.4.1.7. *In-silico* docking interaction of hub targets and key myco-metabolites

After analyzing protein-protein interaction and enrichment analysis of target genes, some of the influential hub target genes involved in the KEGG pathway of cancer were selected for studying structure-based design. The dock results of hub target genes EGFR (PDB Id: 6LUD), ESR1 (PDB Id: 6W0K), MAPK1 (PDB Id: 7M0Y), BCL2L1 (PDB Id: 4LVT) and AKT1 (PDB Id: 4EKL) with their respective EFPO1 myco-metabolites is tabulated in Table 5.6. and pictorially demonstrated in Figure 5.7.

Table 5.6. Docking scores of hub target genes with their respective EFPO1 myco-metabolites.

	EGFR (PDB Id: 6LUD)	**ESR1 (PDB Id: 6W0K)**	**MAPK3 (PDB Id: 7M0Y)**	**BCL2L1 (PDB Id: 4LVT)**	**AKT1 (PDB Id: 4EKL)**
CEP		**-7.2**	**-7.0**		
SEN		-6.8			
LUT	**-7.9**	-6.8			-6.1
KAM	-7.6	-6.5			**-8.0**
QE	-7.8				-6.2
API	-7.6				
PA				**-6.5**	

Bold signifies the maximum score among each class of target genes.

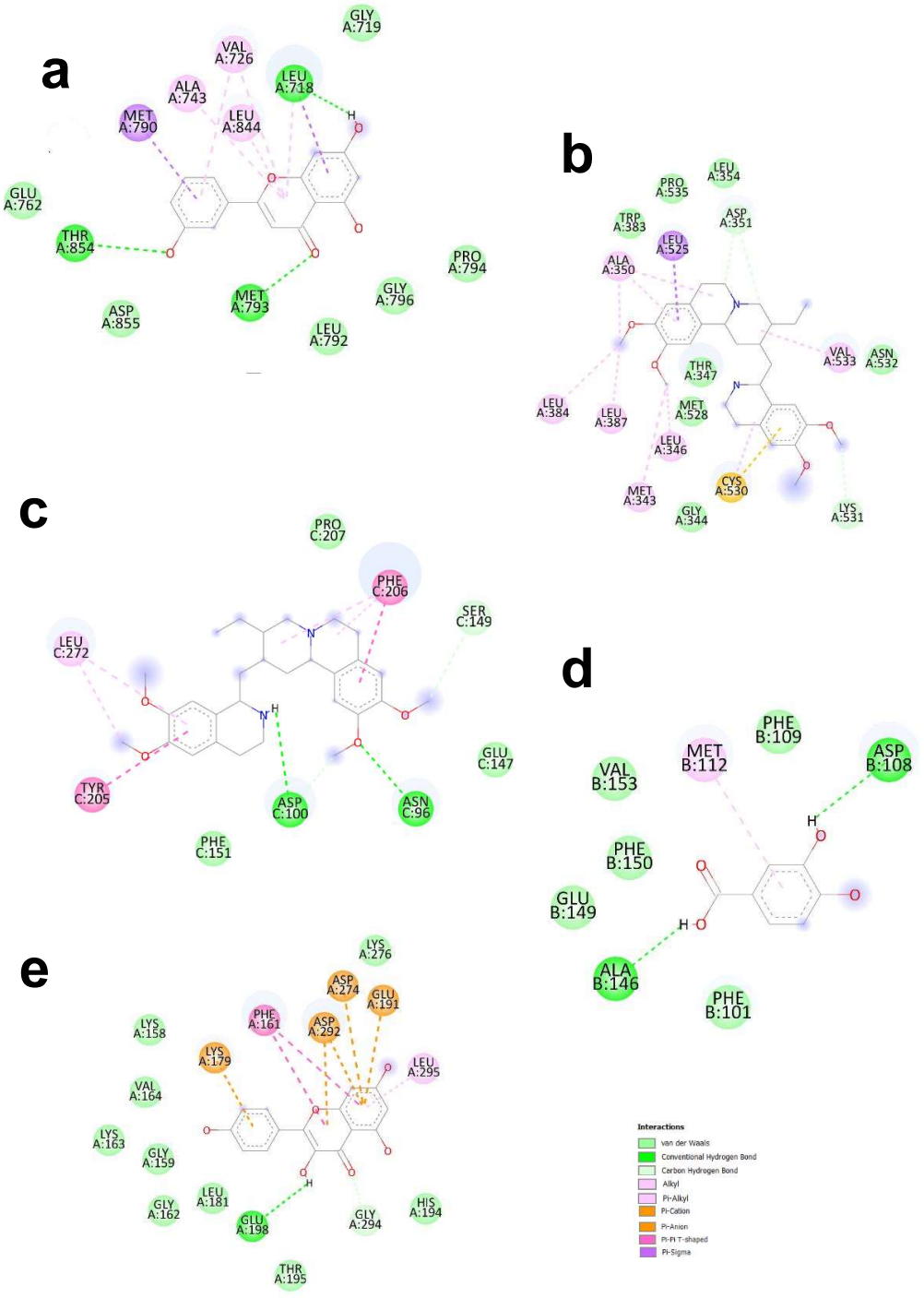

Figure 5.7. Molecular docking analysis of EFPO1 myco-metabolites with their respective target gene (a) LUT and EGFR (PDB Id: 6LUD) (b) CEP and ESR1 (PDB Id: 6W0K) (c) CEP and MAPK3 (PDB Id: 7M0Y) (d) PA and BCL2L1 (PDB Id: 4LVT), and (e) KAM and AKT1 (PDB Id: 4EKL).

5.4.1.8. *In-silico* cancer multi-omic expression study & prognostic potential of selected hub target

GEPIA webserver was used for transcriptional expression study of hub genes among tumor and normal samples. The selected hub target BCL2L1 was highly expressed in lung adenocarcinoma samples as compared to normal tissue ($p < 0.05$) (Figure 5.8 a). Using the UCALAN web server, the protein expression of BCL2L1 was assessed for lung adenocarcinoma patients. BCL2L1 were significantly highly expressed in tumour sample as compared to normal sample ($p < 0.05$) (Figure 5.8.b). For exploring prognostic potential of hub target for lung cancer, UALCAN webserver was used, analyse relationship of mRNA expression of the hub target with the overall survival (OS). As shown in Figure 5.8.c, low mRNA levels of BCL2L1 showed a good prognosis in breast cancer.

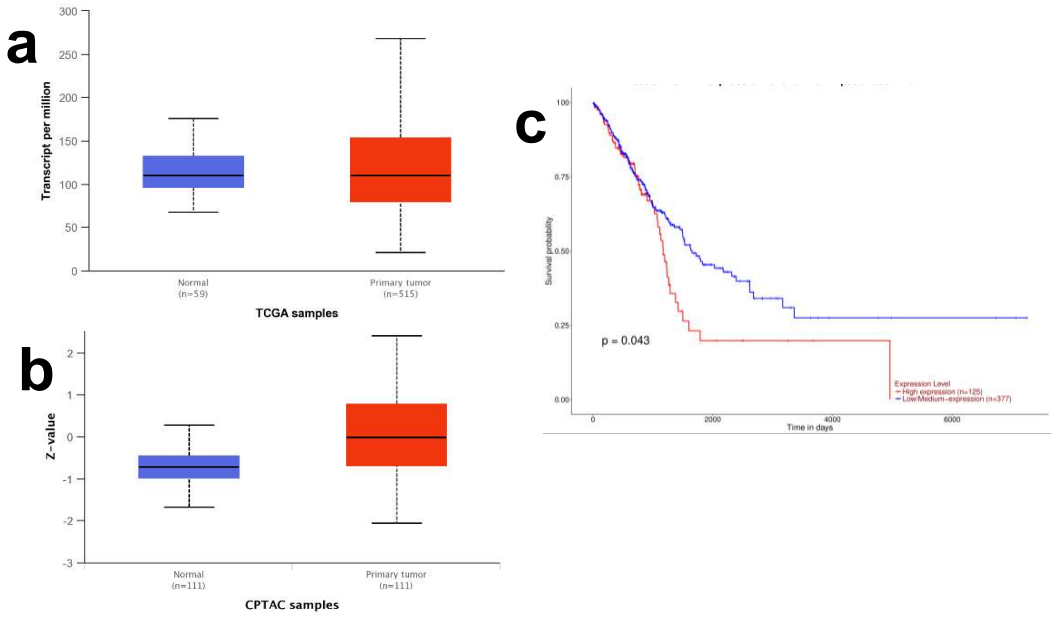

Figure 5.8. *In-silico* cancer multi-omic expression study and prognostic potential of selected hub target BCL2L1 in lung adenocarcinoma patients (a) genomic expression (b) proteomic expression, and (c) overall survival analysis.

5.4.2. *In-vitro* experimental validation

5.4.2.1. Fluorescence microscopy

Morphological alterations at a nuclear level were visually inspected by fluorescence microscopy using nuclear staining dye DAPI. DAPI stained fluorescent photo micrograph clearly demonstrates (Figure 5.9.) a dose-dependent blebbing, nuclear fragmentation, and chromatin condensation of the treated cell, thus indicating induction of apoptosis.

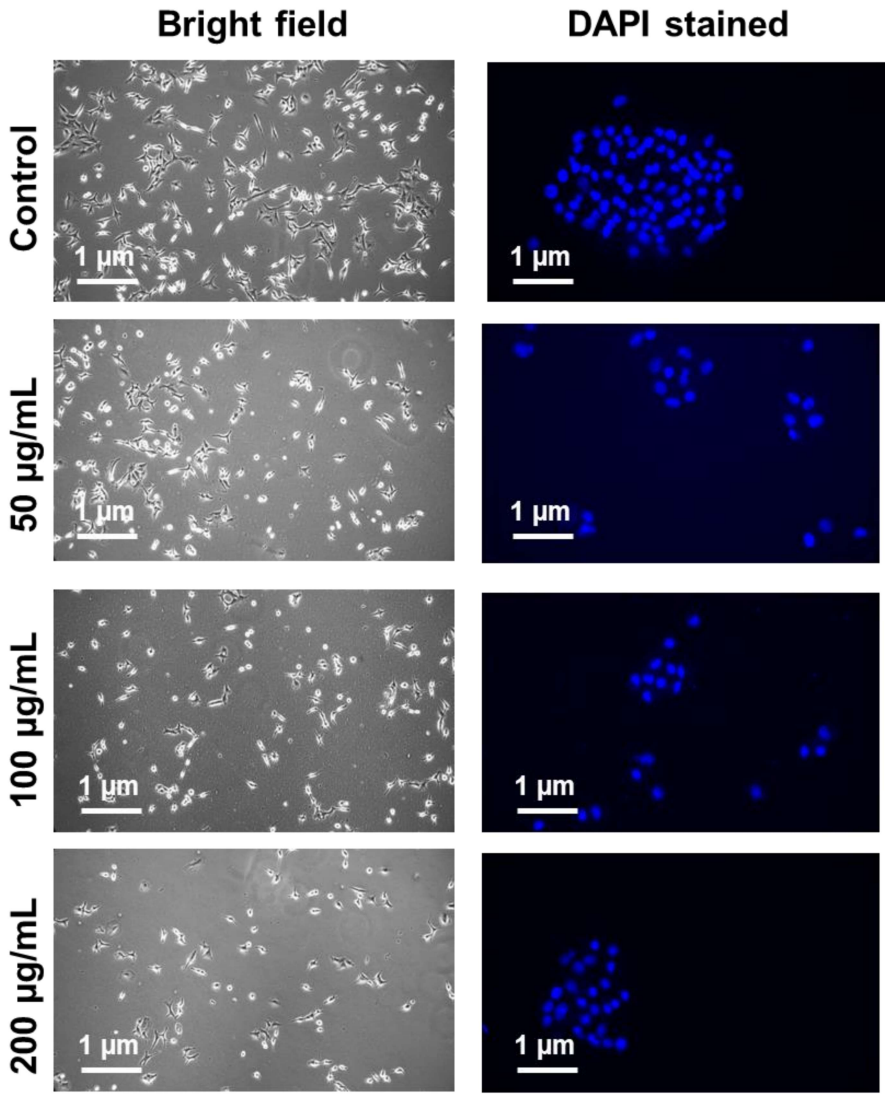

Figure 5.9. Fluorescence micrographs (DAPI stained) of untreated and treated A549 cancer cell line with EFPO1 (0-200 µg/mL). Scale bar: 1µm; Magnification: 20X.

5.4.2.2. Immunoblot analysis

Out of 90 target genes, 44 genes were linked to 'pathway in cancer' by KEGG pathway analysis. These 44 genes were majorly related to estrogen signalling pathway, PPAR signalling pathway, tyrosine kinase signalling pathway, downstream signalling pathway: the MAPK pathway, PIK3-AKT pathway, JAK-STAT pathway, Wnt signalling pathway, CDK, and Bcl-2/Bcl-XL. Whereas, from PPI interaction by STRING webserver, AKT1, VEGFA, EGFR, SRC, ESR1, JUN, ERBB2, PIK3CA, MAPK1, and BCL2L1 were the hub target protein. Hence, to verify the reliability of obtained targets in network pharmacology, immunoblot analysis for BCL2L1, and BAX protein was carried out to trace the signalling pathway involved in the anti-cancer potential of EFPO1. There was a dose-dependent decrease in BCL2L1 expression and increase in BAX expression in EFPO1 treated A549 cell line, as evident in Figure 5. 10. Concluding, EFPO1 anticancer potential is due to the suppression of the BCL2L1 expression.

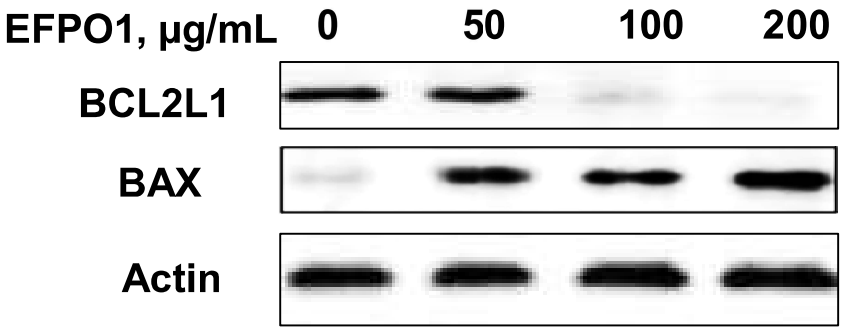

Figure 5.10. Immunoblot analysis using antibodies against BCL2L1, and BAX protein in EFPO1 treated A549 (0-200 µg/mL).

5.4.3. *In-vivo* experimentation

5.4.3.1. Acute toxicity assessment

The acute toxicity of EFPO1 was studied according to OECD 425 guidelines. At the doses of 2000 mg/kg, mortality was observed in Swiss albino mice. The remaining mice surviving 550 mg/kg were further observed for 14 days, and on the 15th day, they were humanely killed, and blood was collected for hematological and biochemical analysis. The biochemical and hematological parameters of surviving mice showed a non-significant difference from control mice ($p < 0.05$), as shown in Table 5.7. and Table 5.8., respectively. The difference in weight of mice on the 0th and 14th day was non-significant (Table 5.9.). No difference in histology architecture was seen in liver and kidney of 550 mg/kg EFPO1 with respect to control mice, as reflected in Figure 5.11. The estimated LD_{50} determined from AOT425statpgm software was 550 mg/kg in Swiss albino mice, attached in *Appendix* (Figure A7).

Table 5.7. Biochemical parameters of EFPO1 (550 mg/kg) group against control Swiss albino mice for acute toxicity assessment.

Biochemical parameters	Control group	EFPO1 (550 mg/kg)
Glucose (mg/dL)	83. 257 ± 4.369	81.738 ± 5.789
SGPT (U/L)	46.768 ± 3.879	48.327 ± 4.018
SGOT(U/L)	140.326 ± 6.256	143.356 ± 4.139
ALP(U/L)	38.523 ± 1.716	41.342 ± 1.248
Total protein (g/dL)	5.013 ± 0.738	4.975 ± 0.583
Urea (mg/dL)	46.231± 2.167	48.365 ± 4.782
Creatinine (mg/dL)	0.423± 0.035	0.661 ± 0.029
Triglyceride(mg/dL)	111.283 ± 5.463	119.273 ± 6.953
Cholesterol (mg/dL)	83.172 ± 4.357	79.654 ± 7.138

Values are expressed as Mean ± SD (n = 3). One-way ANOVA was performed, followed by the turkey's multiple comparison test ($p < 0.05$), using Graph pad prism 5.0.

Table 5.8. Hematological parameters of EFPO1 (550 mg/kg) group against control Swiss albino mice group for acute toxicity assessment.

Hematological parameters	Control group	EFPO1 (550 mg/kg) group
Hemoglobin	10.235±2.647	8.725±1.137
WBC (White blood cell) (*10^3/µl)	9.436±1.243	10.376±1.374
RBC (Red blood cell) (*10^6/µl)	5.237±2.753	4.973±2.073
Packed Cell Volume (HCT) (%)	40.137±3.827	39.261±4.137
Mean Corpuscular Volume (MCV) (fL)	50.745±5.183	45.292±3.392
Mean Corpuscular Hemoglobin (MCH) (pg)	30.735±3.438	31.682±3.896
Mean Corpuscular Hemoglobin Conc. (%)	34.751±2.276	30.843±2.056
RDW (%)	15.428±2.423	14.861±2.513
Platelets Count (*10^5/µl)	6.873±3.728	6.626±3.803

Values are expressed as Mean ± SD (n = 3). One-way ANOVA was performed followed by the turkey's multiple comparison test ($p < 0.05$), using Graph pad prism 5.0.

.

Table 5.9 Change in weight (g) of EFPO1 (550 mg/kg) group in Swiss albino mice for acute toxicity assessment.

	0^{th} day	14^{th} day
Body weight (g)	24.204 ± 1.80	26.746 ± 2.509

Values are expressed as Mean ± SD (n = 3). One-way ANOVA was performed followed by the turkey's multiple comparison test ($p < 0.05$), using Graph pad prism 5.0.

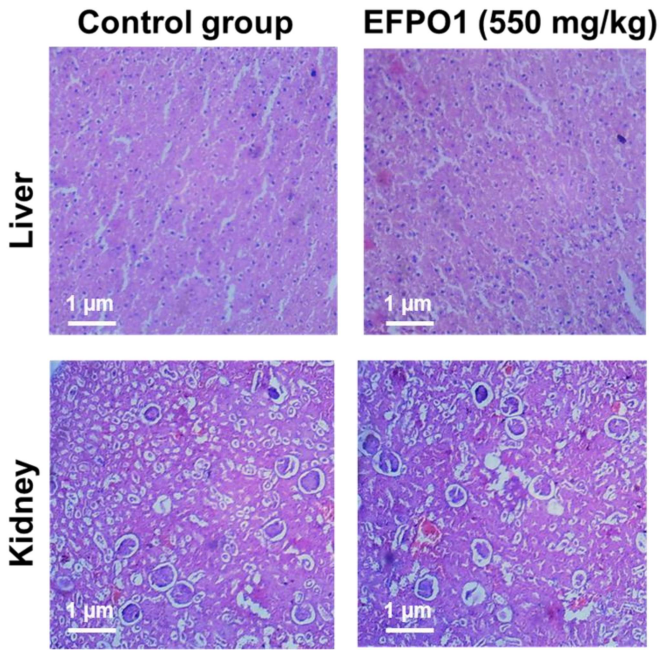

Figure 5.11. Histopathological examination of liver and kidney of EFPO1 (550 mg/kg) group against control Swiss albino mice group for acute toxicity assessment. Scale bar: 1µm; Magnification: 10X.

5.4.3.2. *In-vivo* anti-tumor efficacy in EAC (solid tumor) bearing Swiss albino mice

A reduction in tumor size, tumor volume, and tumor weight of EAC (solid tumor) bearing Swiss albino mice are indicative of *in-vivo* therapeutic efficacy. As compared to be tumor-bearing mice 'T' with tumor volume (980.403 ± 53.211 mm^3), the tumor volume of treated groups E1, E2, E3, and S were measured at approximately 553.452 ± 44.520 mm^3, 385.607 ± 56.050 mm^3, 356.578 ± 73.642 $mm^3$and 83.755 ± 38.026 mm^3 respectively, thus indicating a significant difference ($p < 0.05$) (Figure 5.12.a). Similarly, there was a significant reduction in tumor weight in the treated groups E1, E2, E3, and S (Figure 5.12.b), in contrast to tumor-bearing mice 'T'. The average tumor growth inhibition index of the treated groups E1, E2, E3, and S was found to be 43.549 %, 60.66 %, 63.63%, and 91.46%, respectively, as reflected in Figure 5.12.c. The reduction in tumor volume of the treated group as compared to the untreated group is pictorially represented in Figure 5.12.d. Amongst the treated group, a significantly higher reduction in tumour volume and tumour weight was observed with S group, followed by E2, and E3 ($p < 0.05$). Biochemical parameters (glucose, SGPT, SGOT, ALP, Urea, Creatinine, Cholesterol, and total triglycerides) were in accordance with the control mice, thus indicating non-toxicity, as shown in Table 5.10. Contrarily, a significant difference was observed in the biochemical parameters (glucose, SGPT, SGOT, ALP, urea, cholesterol, and triglycerides) of tumor-bearing mice as compared to the treated and control group. Further, Non-significant differences in the weight of control, tumor-bearing mice, and treated mice on the 0^{th} day and 15^{th} day were observed, as reflected in Table 5.11. No mortality was observed during treatment. With the presented result, EFPO1 can be identified as safe and efficacious in anti-tumor activity, in a dose of 75 mg/kg and 100 mg/kg against EAC (solid tumor) bearing Swiss albino mice.

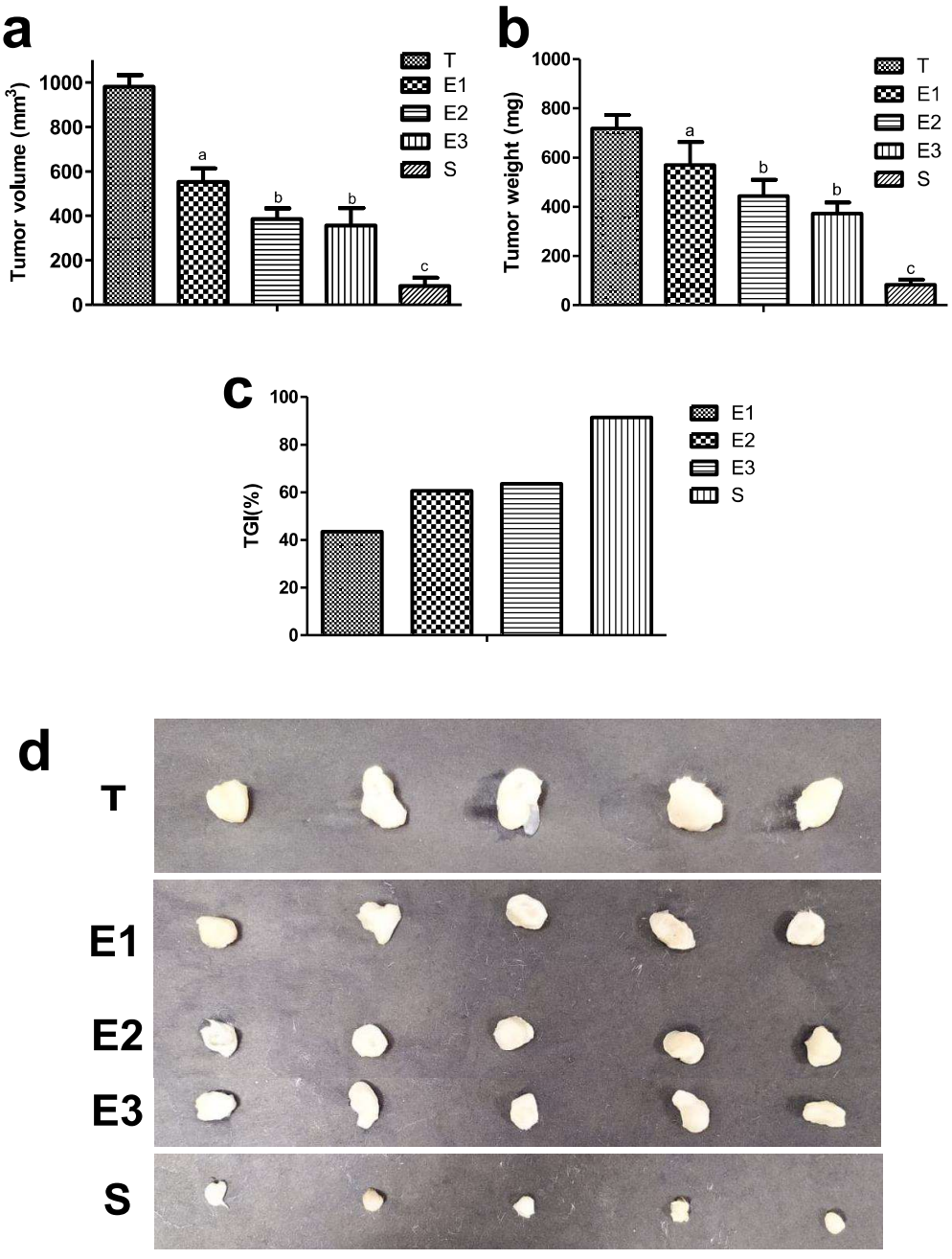

Figure 5.12. *In-vivo* anti-tumor efficacy in EAC (solid tumor) bearing Swiss albino mice. Values are expressed as Mean ± SD (n = 5). One-way ANOVA was performed followed by the turkey's multiple comparison test ($p < 0.05$). Different letters (a, b, and c) represent a significant difference at $p < 0.05$ & same letters represent absence of significant difference.

Table 5.10. Biochemical parameters of control group, tumor-bearing mice group (T), and treated group (E1, E2, E3, and S) of tumor-bearing mice.

Biochemical parameters	Control	T	E1	E2	E3	S
Glucose (mg/dL)	85.3 ± 3.267	126.716 ± 3.46***	83.35 ± 2.428	86.243 ± 3.334	81.625 ± 2.428	89.159 ± 4.028
SGPT (U/L)	43.172 ± 2.428	63.852 ± 7.104***	47.148 ± 7.511	45.654 ± 7.464	38.354 ± 2.546	38.071 ± 2.254
SGOT(U/L)	136.243 ± 3.484	159.812 ± 4.664***	145.258 ± 3.154	143.022 ± 6.849	144.463 ± 5.287	141.384 ± 7.163
ALP(U/L)	37.4868 ± 4.463	65.873 ± 5.698***	45.316 ± 4.498	41.756 ± 3.041	43.276 ± 2.548	42.498 ± 3.954
Urea (mg/dL)	46.657 ± 5.156	70.156 ± 4.498***	48.465 ± 5.924	53.451 ± 2.432	45.435± 4.553	44.753 ± 4.214
Creatinine (mg/dL)	0.435 ± 0.084	1.684 ± 0.0435	0.343 ± 0.043	0.376 ± 0.0123	0.383 ± 0.043	0.428 ±0.054
Triglyceride(mg/dL)	115.014 ± 5.826	139.565 ± 5.368***	120.433 ± 5.232	113.037 ± 5.42	118.235 ± 5.943	120.498 ± 3.498
Cholesterol (mg/dL)	85.5 ± 3.463	110.431 ± 3.517***	80.33 ± 4.527	85.462 ± 5.483	81.485 ± 3.465	86.54 ± 4.356

Values are expressed as Mean ± SD (n = 5). One-way ANOVA was performed followed by the turkey's multiple comparison test ($p < 0.05$), using Graph pad prism 5.0. *** represent a significant difference at $p < 0.05$

Table 5.11. Change in weight (g) of control group, tumor-bearing mice group (T), and treated group (E1, E2, E3, and S) of tumor-bearing mice.

Groups	Body weight (g)	
	0^{th} day	**15^{th} day**
Control	25.426 ± 3.983	27.170 ± 1.320
T	25.521 ± 3.732	26.376 ± 3.241
E1	25.902±2.391	26.783±1.567
E2	24.897±2.919	25.505±2.258
E3	25.425±1.664	27.199±3.754
S	24.383±3.250	25.263±2.861

Values are expressed as Mean ± SD (n = 5). One-way ANOVA was performed followed by the turkey's multiple comparison test ($p < 0.05$), using Graph pad prism 5.0.

5.5. Summary

The overlapping target genes of myco-metabolites-target and disease-target are displayed in Figure 5.1. These are the influential target genes of myco-metabolites of EFPO1, for cancer disease. For the treatment and management of breast and prostate cancer, endocrine therapy/hormonal therapies are used. Through network analysis of PPI interaction (Figure 5.2.), ESR1 (Estrogen receptor 1) was identified as one of the hub target genes with a high number of interactions. Compounds CEP, SEN, LUT, and KAM targets ESR1 target protein (Figure 5.6.). Despite positive outcomes and increased survival rates to treatments, resistance to such hormonal therapies develops. This estrogen receptor can cross-talk with various receptor tyrosine kinases (RTKs) like EGFR, FGFR, and HER. Hence, molecular signalling through the participation of redundant or alternative RTKs such as EGFR, FGFR, and HER can lead to the reactivation of ER- regulated transcription programs and tumor cell growth. Based on a topological feature assessment of protein-protein interaction target genes, EGFR (a member of the RTKs family), was identified as one of the hub target genes (Figure 5.2.) and a probable target for LUT, KAM, QE, and API compounds (Figure 5.6.). In the presented studies, there were other members of the RTKs family, such as ERBB2, IGFR, FGFR, and c-KIT, identified as target genes for the tentative compound identified (Figure 5.6.). Resistance to EGFR-targeted therapy can still be developed due to the activation of other complementary RTKs members and downstream PI3K-AKT and Ras-MEK-ERK pathways (Luo & Fu, 2014)(Ludovini et al., 2011). In the current study, PIK3CA, and AKT1 were illustrated as one of the prominent target proteins with maximum interaction in protein-protein networking (Figure 5.2.); this protein was a probable target for SEN and LUT, KAM, and QE compound, respectively (Figure 5.6.). Whereas CEP myco-metabolite targets MAPK3 (Figure 5.6.), one of the potential hub targets identified

in protein-protein interaction (Figure 5.2.). Pro- and anti-apoptotic BCL-2 protein family members regulate a cell's ability to undergo mitochondrial apoptosis. The balance of pro- and anti-apoptotic BCL-2 proteins enables efficient control of programmed cell death during development. The BCL-2 family, when imbalanced balance, can promote the growth of tumors and cancer therapy resistance while functioning as a roadblock to apoptosis. In the current framework of protein-protein interaction, BCL2L1, notified as one of the prime target proteins with the highest number of edges (Figure 5.2.), was a target for PA (Figure 5.6.).

Over and above this, EFPO1 myco-metabolites also targets PPAR signalling pathway, Wnt signalling pathway, JAK/STAT pathway, and CDK. Synergistically, besides targeting multiple key signalling pathways involved in cancer, EFPO1 myco-metabolites also targets compensatory and redundant pathway, thus overcoming drug resistance.

The top KEGG pathway (Figure 5.4 and Figure 5.5.) describes the importance of 90 target genes involved in the cancer pathogenesis, particularly estrogen signalling pathway, PPAR signalling pathway, tyrosine kinase signalling pathway, downstream signalling pathway: the MAPK pathway, PI3K-AKT pathway, and JAK-STAT pathway, Wnt signalling pathway, CDK, and BCL-2/BCL-XL. Gene ontology's top biological process, cellular component, and molecular function were protein phosphorylation, receptor complex, and protein kinase activity, respectively. Altogether, the above-described gene ontology was related to the RTK family member (Figure 5.3.), a key player involved in the KEGG pathway of cancer, modulating multiple downstream signalling pathways like Ras/Raf/Mek pathway, PI3K/AKT/mTOR pathway, and JAK/STAT.

In addition to this, the docking study further validates target prediction. Hub targets showed a good binding affinity with their respective EFPO1 myco-metabolites (Figure 5.7.). On the basis of the results obtained from network pharmacology, cancer multi-omics approach, and prognostic potential of selected hub target (Figure 5.8.), immunoblot analysis of BCL2L1 were investigated. Results signify evidence of apoptotic bodies from fluorescence microscopy (Figure 5.9.), modulation of BCL2L1 signalling pathway (Figure 5.10.), and a significant decrease in tumor volume and tumor weight of EFPO1 treated EAC bearing Swiss albino mice (Figure 5.12.).

Collectively, this study scientifically traces the anti-cancer mechanistic approach of EFPO1 through network pharmacology, *in-vitro* immunoblot analysis, and *in-vivo* anti-tumor activity.